Monthly Notices
of the
ROYAL ASTRONOMICAL SOCIETY

Mon. Not. R. Astron. Soc. (2010) doi:10.1111/j.1365-2966.2010.17757.x

The γ-ray binary LS 5039: mass and orbit constraints from *MOST* observations⋆

Gordon E. Sarty,[1,2]† Tamás Szalai,[3] László L. Kiss,[4,5] Jaymie M. Matthews,[6] Kinwah Wu,[5,7] Rainer Kuschnig,[8] David B. Guenther,[9] Anthony F. J. Moffat,[10] Slavek M. Rucinski,[11] Dimitar Sasselov,[12] Werner W. Weiss,[8] Richard Huziak,[1] Helen M. Johnston,[5] Andre Phillips[13] and Michael C. B. Ashley[13]

[1]*Royal Astronomical Society of Canada, Saskatoon Centre, PO Box 317, RPO University, Saskatoon, SK S7N 4J8, Canada*
[2]*Department of Physics and Engineering Physics, University of Saskatchewan, Saskatoon, SK S7N 5E2, Canada*
[3]*Department of Optics and Quantum Electronics, University of Szeged, Dóm tér 9., Szeged H-6720, Hungary*
[4]*Konkoly Observatory of the Hungarian Academy of Sciences, PO Box 67, H-1525 Budapest, Hungary*
[5]*Sydney Institute for Astronomy, School of Physics A28, University of Sydney, NSW 2006, Australia*
[6]*Department of Physics and Astronomy, University of British Columbia, 6224 Agricultural Road, Vancouver, BC V6T 1Z1, Canada*
[7]*Mullard Space Science Laboratory, University College London, Holmbury St. Mary, Dorking, Surrey RH5 6NT*
[8]*Institut für Astronomie, Universität Wien, Türkenschanzstrasse 17, A-1180 Vienna, Austria*
[9]*Department of Astronomy and Physics, Saint Mary's University, Halifax, N.S., B3H 3C3, Canada*
[10]*Observatoire Astronomique du Mont Mégantic, Département de Physique, Université de Montréal C. P. 6128, Succursale: Centre-Ville, Montrèal, QC H3C 3J7, Canada*
[11]*Department of Astronomy and Astrophysics, University of Toronto, Toronto, ON M5S 3H4, Canada*
[12]*Harvard–Smithsonian Center for Astrophysics, 60 Garden Street, Cambridge, MA 102138, USA*
[13]*School of Physics, Department of Astrophysics and Optics, University of New South Wales, Sydney, NSW 2052, Australia*

Accepted 2010 September 22. Received 2010 September 21; in original form 2010 May 11

ABSTRACT

The results of a coordinated space-based photometric and ground-based spectroscopic observing campaign on the enigmatic γ-ray binary LS 5039 are reported. 16 d of observations from the *MOST* satellite have been combined with high-resolution optical echelle spectroscopy from the 2.3-m ANU Telescope in Siding Spring, Australia. These observat ions were used to measure the orbital parameters of the binary and to study the properties of stellar wind from the O primary. We found that any broad-band optical photometric variability at the orbital period is below the 2 mmag level, supporting the scenario that the orbital eccentricity of the system is near the 0.24 ± 0.08 value implied by our spectroscopy, which is lower than values previously obtained by other workers. The low amplitude optical variability also implies the component masses are at the higher end of estimates based on the primary's O6.5V((f)) spectral type with a primary mass of $\sim$26 $M_\odot$ and a mass for the compact star of at least 1.8 $M_\odot$. The mass-loss rate from the O primary was determined to be 3.7 to 4.8 $\times$ 10^{-7} $M_\odot$ yr^{-1}.

Key words: stars: binaries: close – circumstellar matter – stars: individual: LS 5039.

1 INTRODUCTION

LS 5039 (V479 Sct) is the optical counterpart of the peculiar X-ray source RX J1826.2−1450 (Motch et al. 1997). The system has been observed in the radio, optical/infrared (optical/IR), ultraviolet (UV), X-ray and γ-ray wavelengths. A radio counterpart has been identified in VLA observations by Martí et al. (1998). The emission appeared to be persistent and was non-thermal. A pair of symmetric radio features were later found associated with the source (core) in VLBA observations by Paredes et al. (2000, 2002), which were interpreted as emission from two opposite relativistic jets. The system was also identified with a very high energy (VHE) γ-ray source found in the *Compton Gamma-ray Observatory*/EGRET (*CGRO*/EGRET) (Paredes et al. 2000) and HESS (Aharonian et al. 2005a) surveys. The detection of MeV–GeV/TeV emission placed LS 5039/RX J1826.2−1450 into a class of unusual high-energy

⋆Based on data from the *MOST* satellite, a Canadian Space Agency mission, jointly operated by Microsat Systems Canada Inc. (MSCI, formerly the space division of Dynacon Inc.), the University of Toronto Institute for Aerospace Studies and the University of British Columbia, with the assistance of the University of Vienna.

†E-mail: gordon.sarty@usask.ca

objects, the γ-ray binaries. So far, only a handful of γ-ray binaries are known. The others are PSR B1259−63 (Aharonian et al. 2005b), LS I +61 303 (Albert et al. 2006; Acciari et al. 2008), Cygnus X–1 (Albert et al. 2007), Cygnus X–3 (Tavani et al. 2009), and the recent candidate HESS J0632+057 (Hinton et al. 2009).

LS 5039/RX J1826.2−1450 (hereafter, referred to as LS 5039) has been classified as a high-mass X-ray binary in the catalogue compiled by Liu, van Paradijs & van den Heuvel (2006). The distance to the source is ≈2.5 kpc (Casares et al. 2005). Its primary is a bright ($V = 11.2$) massive O star (Clark et al. 2001; McSwain et al. 2001), and its secondary is a compact star. It is still a matter of debate whether the compact star in LS 5039 is a black hole or a neutron star. UV and optical spectroscopy established that the primary is a O6.5V((f)) star (McSwain et al. 2004). The presence of P Cygni profiles in the UV N v λ1240 and C iv λ1550 lines (McSwain et al. 2004) indicates a strong wind outflow, whose rate has been estimated to be $\sim 10^{-7}\,M_\odot\,yr^{-1}$ or even higher (McSwain et al. 2004). From the radial velocities of the Hα and He lines, McSwain et al. (2004) (hereafter M04) obtained an orbital period $P = (4.4267 \pm 0.0005)$d and derived the mass function $f(m) = (0.0017 \pm 0.0005)\,M_\odot$, the orbital eccentricity $e = 0.48 \pm 0.06$ and $a_1 \sin i = (1.36 \pm 0.13)\,R_\odot$, where a_1 is the semi-major axis of the primary's orbit and i is orbital inclination. They argued that the mass of the primary O star is in the range (20–35) $M_\odot$, and the compact secondary is a neutron star which has a mass ≈1.4 $M_\odot$. Casares et al. (2005) (hereafter C05) conducted a comprehensive analysis of the optical H Balmer and He i and He ii lines and obtained $P = (3.90603 \pm 0.00017)$d, $e = 0.35 \pm 0.04$, $f(m) = (0.0053 \pm 0.0009)\,M_\odot$ and $a_1 \sin i = (1.42 \pm 0.07)\,R_\odot$. They derived that the orbital inclination $i = (24.9 \pm 2.8)^\circ$, the primary O star has a mass $M_1 = 22.9^{+3.4}_{-2.9}\,M_\odot$ and the compact star has a mass $M_2 = 3.7^{+1.3}_{-1.0}\,M_\odot$. The orbital period obtained by C05 is shorter than that obtained by M04. It is however consistent with the modulations observed in the X-rays (Bosch-Ramon et al. 2005; Takahashi et al. 2009) and γ-rays at GeV (Abdo et al. 2009) and TeV (Aharonian et al. 2006) energies. Aragona et al. (2009) (hereafter A09) revisited radial velocity (RV) measurements from optical spectra, confirming the 3.9-d orbital period. Their refined orbital parameters are $P = (3.90608 \pm 0.00010)$d, $e = 0.337 \pm 0.036$, $f(m) = (0.00261 \pm 0.00036)\,M_\odot$ and $a_1 \sin i = (1.435 \pm 0.066)\,R_\odot$.

One major question about LS 5039 is the nature of the compact object. The orbital parameters derived by C05 clearly indicate that the compact star has a mass exceeding 3.0 $M_\odot$, the usually accepted upper limit of masses of neutron stars (Lattimer & Prakash 2007), implying that LS 5039 is a candidate black hole high-mass X-ray binary. Black hole binaries with a massive O-type donor star are very rare, partly because of the extremely short life-spans of such systems. To date, Cyg X–1 is the only known black hole X-ray binary in the Milky Way with a massive O donor star. The presence of a black hole or not in LS 5039 would therefore have significant implications not only on the formation of black hole high-mass X-ray binaries and the population of such systems in the Milky Way, but also on how very high energy (TeV) emission is produced in γ-ray binaries (see e.g. Araudo, Bosch-Ramon & Romero 2009).

The issue of the nature of the compact star associated with LS 5039 is far from being settled. While the spectroscopic observations of C05 favour the black hole scenario, some workers have argued for a neutron-star scenario involving a non-accreting young pulsar (Martocchia, Motch & Negueruela 2005; Dubus 2006; Sierpowska-Bartosik & Torres 2007; Cerutti, Dubus & Henri 2008). Observationally, Ribó et al. (2008) found that changes in the *mas* morphology of the radio images were difficult to reconcile with the micro-quasar (black hole binary) scenario in which the radio emission originates from expanding plasmons. The situation is further complicated by the fact that the temporal and spectral behaviour of the X-ray emission (Bosch-Ramon et al. 2007; Kishishita et al. 2009; Takahashi et al. 2009; Bosch-Ramon 2010) and properties of the TeV emission (Bosch-Ramon, Khangulyan & Aharonian 2008; Khangulyan, Aharonian & Bosch-Ramon 2008; Abdo et al. 2009) indicate that the high-energy radiation might originate from regions far outside the binary orbit of LS 5039.

We have been observing LS 5039 photometrically with ground-based telescopes at optical and near IR wavelengths to search for orbital modulation, but orbital variations have not been detected in those data (to be reported elsewhere). However, we have detected variations at the 20 mmag level, especially in the I_C band. This prompted us to take a closer look at the optical photometric variations of LS 5039 from space with the Canadian Microvariability and Oscillations of Stars (*MOST*) satellite. Our *MOST* observations were made in 2009 July, simultaneously with ground-based optical spectroscopic observations from the Australian National University (ANU) 2.3-m Telescope at Siding Spring Observatory, Australia. Here we report on the main findings, especially those concerning the masses of the component stars in LS 5039 and the nature of the compact star.

This paper is organized as follows. In Section 2 we describe the photometric observations with the *MOST* space telescope and the spectroscopic observations with the ANU 2.3-m Telescope, which were made simultaneously. In Section 3 we describe the data analysis, present the results on the system's orbital and other parameters, and discuss the implications of the nature of the compact object and the properties of the wind/outflow from the primary star. The conclusions are summarized in Section 4.

2 SIMULTANEOUS PHOTOMETRIC AND SPECTROSCOPIC OBSERVATIONS

2.1 *MOST* photometry

The *MOST* microsatellite (Matthews et al. 1999; Walker et al. 2003) houses a 15-cm Rumak-Maksutov telescope feeding a CCD photometer through a custom optical broad-band (350–750 nm) filter. From its polar Sun-synchronous orbit (altitude = 820 km; orbital period = 101 min), it has a Continuous Viewing Zone (CVZ) about 54° wide within which it can monitor target fields for up to 2 months without interruption. Targets brighter than $V \sim 6$ are observed in Fabry Imaging mode; fainter targets (like LS 5039) are observed in Direct Imaging mode, similar to standard CCD photometry with a ground-based instrument. The photometry is non-differential, but given the orbit, thermal and design characteristics of *MOST*, experience has shown that it is a very photometrically stable platform even over long time-scales (with repeatability of the mean instrumental flux from a non-variable target of the brightness of LS 5039 to within about 1 mmag).

The science exposures on the *MOST* Science CCD take place at the same time as the guide star exposures for satellite pointing. In the case of the LS 5039 observations, the guide star exposure time (and hence the science target exposure time) was 3.03 s. To build up signal-to-noise ratio (SNR), the science exposures were co-added on board the satellite in 'stacks' of 10 exposures. Stacks (each 30.3 s of total integration) were downloaded from the satellite consecutively (with no dead time between stacks), giving a sampling rate of about twice per minute.

The LS 5039 field lies outside the *MOST* CVZ so it could not be monitored continuously. This field alternated with another *MOST* Primary Science Target field (the Wolf–Rayet star WR 113) during each *MOST* satellite orbit. Typically, we monitored LS 5039 for about 70 per cent of every second *MOST* orbit (or about 70 of every second interval of 101 min) between 2009 July 7 and 23.

Due to the observing season and the location of the LS 5039 field relative to the illuminated limb of the Earth, scattered earthshine was high during the beginning and end of each 'visit' to the LS 5039 field. We truncated about 15–20 min of each orbit from the original data to preserve the highest photometric precision. We also filtered outliers caused by cosmic ray hits, especially during passages of the satellite through the South Atlantic Anomaly (SAA). However, the resulting light curve has an effective duty cycle of about 50 per cent (with gaps at intervals of about 101 min) and it still sampled the important time-scales in the LS 5039 system thoroughly.

2.2 Echelle spectroscopy

The spectroscopic observations were carried out on four nights between 2009 July 8 and 11 (during the *MOST* observations) and on three nights between August 1 and 3, using the ANU 2.3-m Telescope with an echelle spectrograph. In total, 118 spectra were obtained that cover almost 40 h with nearly uniform sampling of the whole orbit. The integration times were between 900 and 1200 s and the spectra covered the whole visual range between 3900 and 6720 Å. The nominal spectral resolving power was $\lambda/\Delta\,\lambda \approx 23\,000$ at the Hα line, with a typical SNR per extracted pixel of about 100 for combined spectra that represented 1-h integrations.

All data were reduced with standard IRAF[1] tasks, including bias and flat-field corrections, cosmic ray removal, extraction of the 27 individual orders of the echelle spectra, wavelength calibration and continuum normalization. ThAr spectral lamp exposures were regularly taken before and after every object spectrum to monitor the wavelength shifts of the CCD spectra. We also obtained spectra for the telluric standard HD 177724 and the O6–7V((f)) spectral template HD 168075 (Dufton et al. 2006). Typical continuum-normalized spectra for LS 5039 and HD 168075 are shown in Fig. 1.

3 DATA ANALYSIS AND RESULTS

3.1 Radial velocities

To measure radial velocities we first generated 1-h long averaged spectra to get higher SNR–1 h corresponds to 0.01 orbital phase, hence negligible phase smearing appears in the phased RV data. Radial velocities of the H I, He I and He II lines were determined by fitting two-component functions (a concentric sum of Gaussian and Lorentzian functions) and calculating the shift of the centroids to laboratory wavelengths. To check our method we also determined the velocities of some interstellar lines (Ca II K, Na I D, DIB λ5780, DIB λ6613) for each night. We applied heliocentric corrections to the RV for each line at each time. The data were phased with an orbital period of 3.906 d (C05). The success in generating a RV curve with this phase folding supports the orbital period of LS 5039 as being that obtained by C05 instead of the longer 4.4-d period obtained by M04.

[1] IRAF is distributed by the National Optical Astronomy Observatories, which are operated by the Association of Universities for Research in Astronomy, Inc., under co-operative agreement with the National Science Foundation.

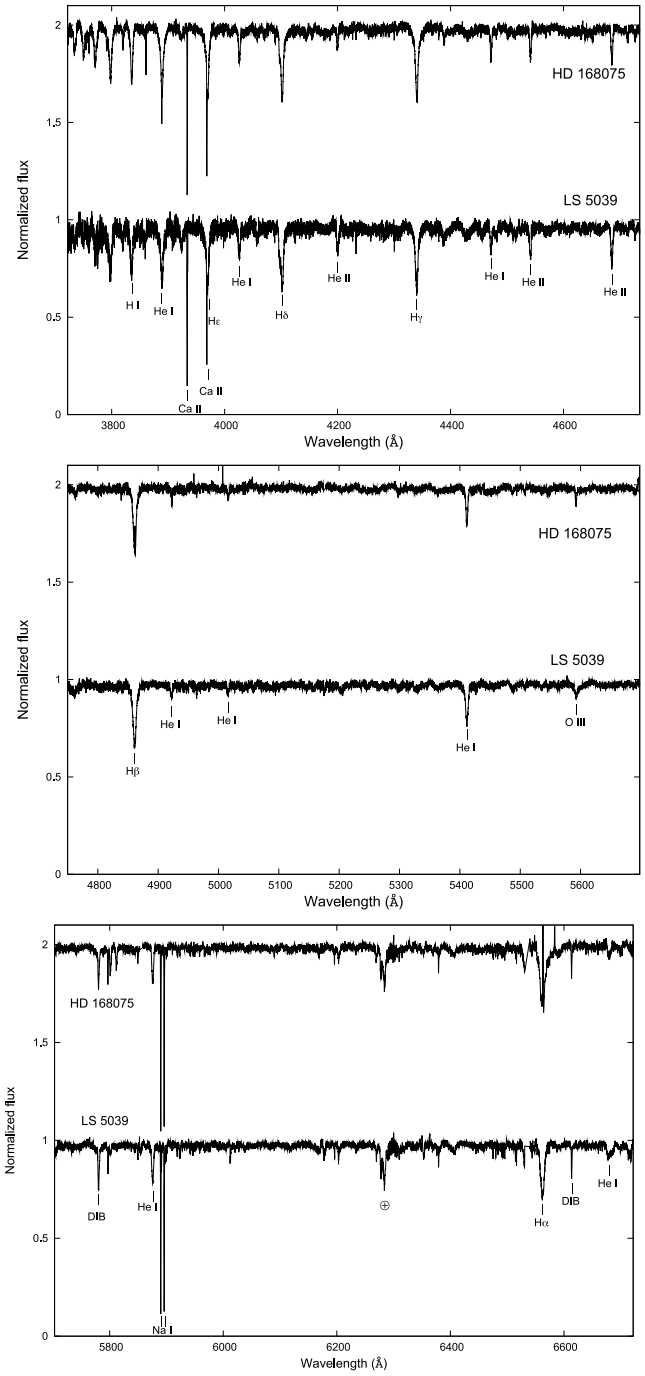

Figure 1. Continuum normalized spectra of LS 5039, classified as type O6.5V((f)), and the O6–7V((f)) spectral template star HD 168075.

To generate the final RV diagrams we used averaged velocities of the H I (Hα, Hβ, Hγ, Hδ, λ3835), He I (λλ4471, 5875) and He II (λλ4200, 4686, 5411) lines; there are several other H and He lines in the wavelength region of our spectra (e.g. the frequently used He II λ4542 line), but they were too noisy or blended to use for velocity determination. The resulting RV diagrams are shown in Fig. 2, top. The error bars shown in Fig. 2 (typically ± 10 to $\pm 15\,\mathrm{km\,s^{-1}}$ in magnitude) represent plus and minus one standard deviation of the measured velocities of two to five lines at different wavelengths. The relatively large errors were caused partly by observational noise and

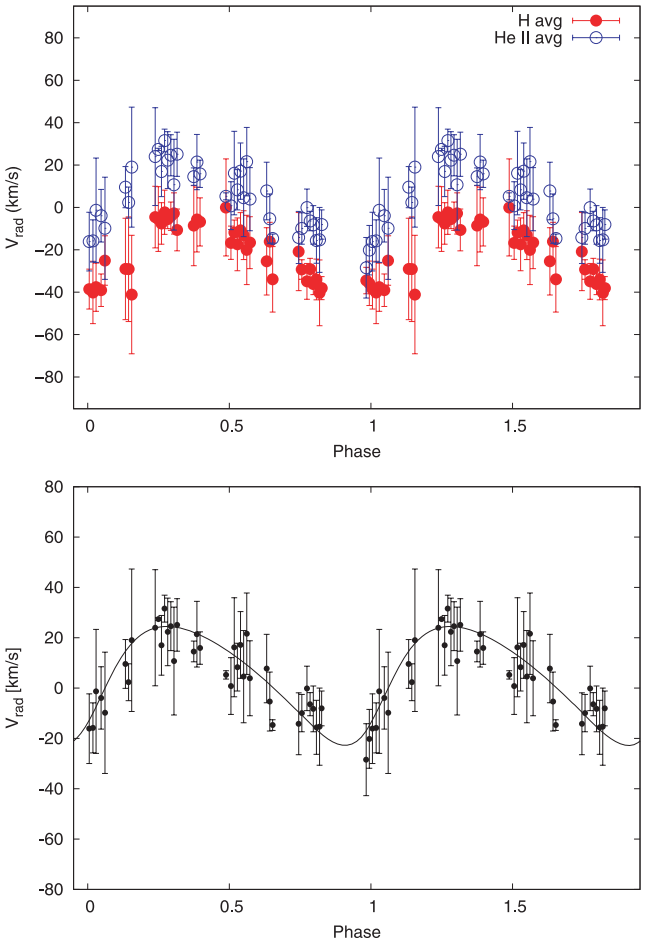

Figure 2. Top: Radial velocities based on H Balmer and He II lines. Bottom: the best-fitting curve to radial velocities of He II lines.

partly by the high rotational velocity of the O star ($v_{\rm rot} \sin i = 113 \pm 8\,{\rm km\,s^{-1}}$, C05).

We detected systematic increasing blueshifts from the He II lines to the He I lines to the H Balmer lines. C05 have also described this effect, but found its degree to be smaller (they obtained an $\sim$8 km s^{-1} shift between the average RVs of the He II and H Balmer lines, as opposed to our 20 km s^{-1} value). We believe that the RV shift is due to the contamination of wind for the He I and H I lines [see Puls et al. (1996)], and so we did not use those two atomic line sets to constrain the orbit.

Additionally, redshifted satellite absorptions were found in the Ca II K and Na I D1 and D2 interstellar absorption lines with a RV around +60 km s^{-1} (more precisely, $+58.4 \pm 2.2\,{\rm km\,s^{-1}}$ by Ca K, $+62.9 \pm 2.3\,{\rm km\,s^{-1}}$ by Na D1 and $+61.9 \pm 1.7\,{\rm km\,s^{-1}}$ by Na D2). These satellite lines may belong to a formerly unknown Galactic Intermediate Velocity Cloud [IVC; see the review by Wakker & van Woerden (1997)].

3.2 Orbital and system parameters

In the following analysis we adopted $T_{\rm eff} = 39\,000 \pm 1000$ K and $\log g = 3.85 \pm 0.10$ for the O primary (C05). We measured the equivalent widths (EW) of several interstellar lines to estimate the interstellar reddening (see Section 3.4 for EW measurements of other lines). Using Na I D1 [EW $= 0.70 \pm 0.02$ Å with the relation to reddening as per Munari & Zwitter (1997)], DIB λ5780 and DIB λ6613 [EW $= 0.55 \pm 0.05$ Å and 0.18 ± 0.02 Å, respectively with the relation to reddening as per Cox et al. (2005)] lines, we found $E(B-V) = 1.2 \pm 0.1$, which is in agreement with previous results [1.25 to 1.35, Ribó et al. (2002) and 1.28 ± 0.02, M04]. Based on this agreement, we adopted the values $d = 2.5 \pm 0.1$ kpc, $M_{\rm O} = 22.9^{+3.4}_{-2.9}\,M_\odot$ and $R_{\rm O} = 9.3^{+0.7}_{-0.6}\,R_\odot$ obtained by C05.

RV curves were modelled using the 2003 version[2] of the Wilson–Devinney (WD) code (Wilson & Devinney 1971; Wilson 1994; Wilson & van Hamme 2003). We used only our own velocity points and did not use previous RV measurements made by others. Our data set therefore represents the highest resolution, homogenous spectral data set yet used to obtain an orbital solution for LS 5039. Given the lack of X-ray eclipses we could not use the special mode in WD code developed for modelling the orbits of X-ray binaries. Therefore, we analysed LS 5039 as a single line spectroscopic binary without any (X-ray) light curves. This limitation allowed us to determine only the mass function, $f(m)$, as a function of different inclination angles, i. We could not determine the exact values of the inclination, i, and the mass ratio, q. However, knowledge of the primary's mass, $M_{\rm O}$, allowed us to narrow the possible parameter space.

As described previously, we adopted the 3.906-d period as a fixed parameter during the modelling. The computed value of $T_0 =$ HJD 2455017.08 was used as the epoch of periastron. The computed orbital parameters are given in Table 1 where they are compared to the results of C05 and A09. The RV curve implied by the solution is shown in Fig. 2, bottom. Our values and the ones published by C05 are based only on velocity points from the He II lines, while A09 applied the velocities of every available H, He I and He II line, a process which combines lines from two different sources on and near the O star as mentioned in Section 3.1.

In general, our computed orbital parameters are close to earlier solutions, but there are some differences. The value of the computed systemic RV, V_γ, was significantly higher (by 15 to 20 km s^{-1}) for each line type (H I, He I and He II) in C05 than what we found. The possibility of a real change in the system RV over a few years is very small, so the cause of the difference is likely due to differences in data analyses.

3.3 Mass of the compact object

One of the main goals of our investigation was to obtain stronger constraints on the mass of the non-stellar companion. C05 executed detailed light curve simulations using their orbital solution for LS 5039; they found that if the inclination angle is around 30°, then photometric variability caused by the distortion of the primary should be of the order of 0.01 mag near periastron. If the change in brightness is 0.01 mag or less then the inclination is 30° or less. An inclination less than 30°, in turn, implies that the mass of the compact object is too high ($>3.0\,M_\odot$, C05) to be a neutron star. Lacking the necessary 2–3 mmag photometric accuracy required, they could not check their scenario.

As described in Section 3.2, our new analysis of the orbital parameters of LS 5039 is based on an independent homogeneous RV data set. Our results are in good agreement with the one presented by C05 – in particular, the values of mass functions, the implications of which are shown in Fig. 3, agree within the uncertainties.

Photometric data from the *MOST* satellite (6649 individual brightness measurements through 16 d between July 7 and 23) did not show any variability greater than a few mmag. To quantify the

[2] ftp://ftp.astro.ufl.edu/pub/wilson

Table 1. Orbital parameters of LS 5039.

Parameter	C05 (He II)	A09	This paper (He II)
T_0 (HJD−2450000)	1943.09 ± 0.10	2825.99 ± 0.05	5017.08 ± 0.06
$P_{\rm orb}$ (d)	3.906 03	3.906 08	3.906 (adopted)
e	0.35 ± 0.04	0.34 ± 0.04	0.24 ± 0.08
ω (°)	225.8 ± 3.3	236.0 ± 5.8	237.3 ± 21.8
V_γ (km s^{-1})	17.2 ± 0.7	4.0 ± 0.3	3.9 ± 1.3
K_1 (km s^{-1})	25.2 ± 1.4	19.7 ± 0.9	23.6 ± 4.0
$a_1 \sin i$ ($R_\odot$)	1.82 ± 0.10	1.44 ± 0.07	1.77 ± 0.15
$f(m)$ ($M_\odot$)	0.0053 ± 0.0009	0.0026 ± 0.0004	0.0049 ± 0.0006
RMS of fit (km s^{-1})	9.1	7.1	6.2

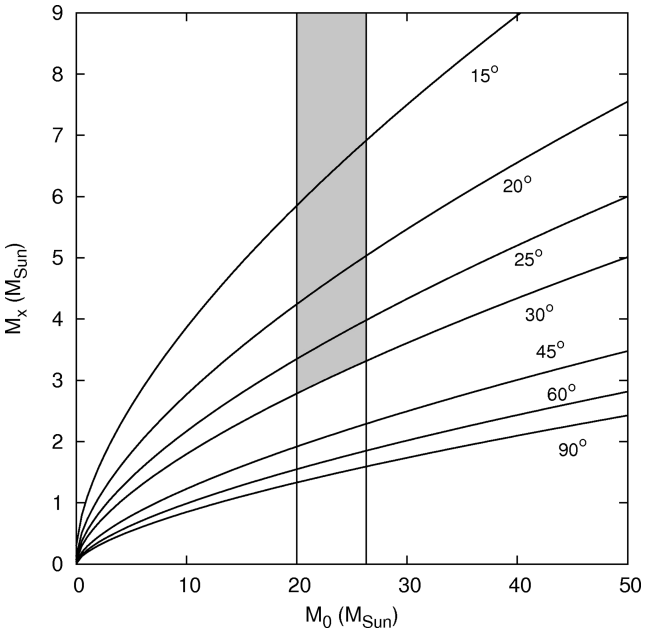

Figure 3. Mass constraints of the two components in LS 5039 for different inclinations from the measured mass function. The vertical lines are the limits of the O-type stellar companion mass adopted from C05. The gray region represents the possible values of the compact object given that the orbital inclination is less than 30°.

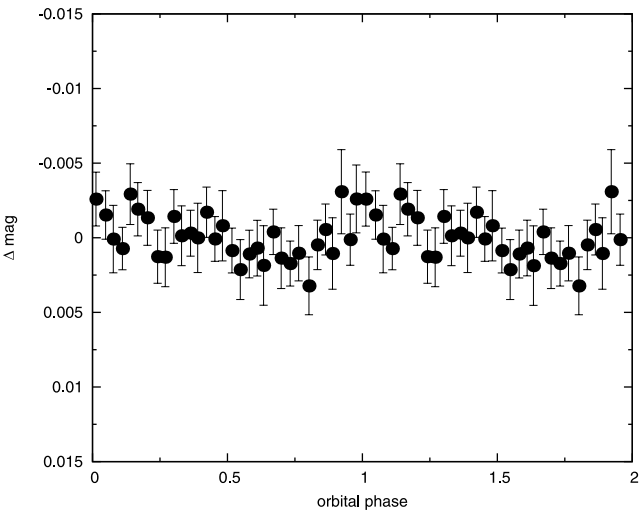

Figure 4. Phase-binned folded light curve from the *MOST* observations. The error bars represent 99 per cent confidence intervals of the mean values computed from $3\sigma/\sqrt{n}$ where σ is the standard deviation and n is the number of data points in a given phase bin. The *MOST* data originally represent fractional change from the mean in terms of flux so a change of sign gives the Δ mag values shown here that represent the magnitude difference from the mean. This conversion of the *MOST* data to Δ mag allows us to directly compare the data to the simulations shown in Fig. 5.

frequency content of the light curve, we performed a period analysis of the full data set using the PERIOD04 software (Lenz & Breger 2004). The resulting frequency spectrum does not contain any significant peak with an amplitude greater than 0.002 mag. Moreover, the orbital period does not jump out of the noise either. As a different approach, we phased the light curve with the spectroscopic period and epoch and used 0.03 phase bins to reveal if there is any optical variability due to orbital motion. Fig. 4 shows the phase-binned folded light curve, which indicates a possible variability at the level of 2 mmag, with an apparent broad minimum at phase $\varphi \sim 0.7$–0.8. Although the SNR of the binned light curve is low for detailed speculations, we compared the shape of the curve with the EW variations of hydrogen and helium lines (see Section 3.4) and with the results of our own light curve simulations.

To check and understand the conclusions of the C05 light curve simulations, we used the WD code to do our own simulations. Two sets of simulated light curves were computed: for the first set the mass of the compact object was fixed to 3.0 $M_\odot$; for the second set the mass of the compact object was determined from the mass function derived from our RV data as described in Section 3.2. In each set, the mass of the primary was set to either 20 or 26 $M_\odot$, the eccentricity was set to either 0.35 or 0.24, the V band was used to approximate the *MOST* band and, inclinations of 60°, 30° and 20° were modelled. The results from the second set of simulations, with the mass function fixed to our measured value, are shown in Fig. 5. For all simulations the primary radius was set to $R_O = 9.5\,R_\odot$ and a linear cosine law (Wilson & van Hamme 2003) was used for limb darkening effects. The compact object was handled as a point source.

The first set of simulations, with the mass of the compact object fixed at 3.0 $M_\odot$, gave light curves that followed the pattern described by C05: the amplitude of the light curve decreased as the inclination decreased. The results with the fixed mass function simulations were different, as seen in Fig. 5: the amplitude of the light curve decreased with increasing total system mass and decreasing eccentricity but did not decrease with decreasing inclination. For fixed system mass and eccentricity the inclination diagnostic is better given by the light curve shape, especially the dip near phase 0, and not by its amplitude. A formal curve fit of the *MOST* data to the light curves of the $M_O = 26\,M_\odot, e = 0.24$ case gave the best fit with an inclination of 60°. However, this result must be viewed as preliminary, at best, because the amplitude difference between the

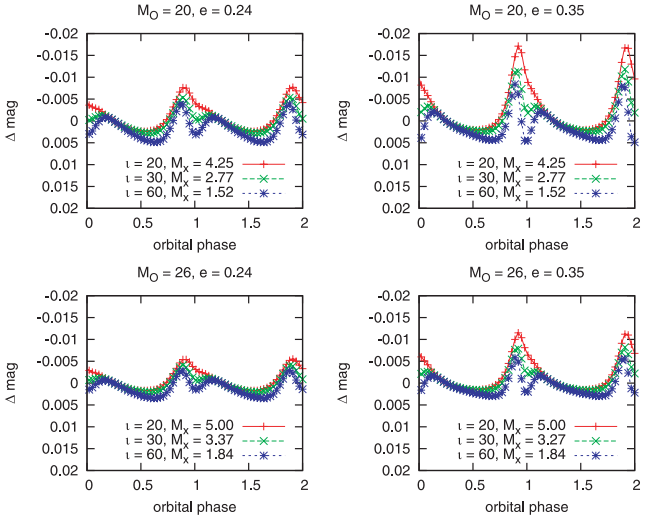

Figure 5. Model light curves. All models have the mass function fixed to $0.0049\,M_\odot$. M_O is the mass of the primary, M_x is the mass of the compact companion. The amplitude of the light curves decrease with increasing system mass and decreasing eccentricity.

different inclination light curves is very small, the binned *MOST* data have considerable scatter at the mmag level, and the effect of the stellar wind and accretion on the light curve are not modelled in the WD code.

We note that some studies suggest the mass of an O6.5V type star to be around 28–29 $M_\odot$ (Martins, Schaerer & Hillier 2005) rather than 20–26 $M_\odot$ used in C05. In the case of a heavier primary, the mass of the compact object would also be larger and the M_x masses shown in Fig. 5 would be greater, strengthening the argument for the black hole nature of the secondary compact star, even at relatively higher inclinations.

3.4 Stellar wind

To infer the mass-loss rate of the O-type star and the properties of the circumstellar matter, we determined the EW of each H and He line and also their variability during the orbit, which could be good indicators of physical processes taking place in the stellar wind. As mentioned in Section 3.2, we also measured the EWs of some other lines to check the value of interstellar reddening given in the literature. We made the measurements on the average of spectra summed to 1-h long exposure times, but we plotted the daily average values of the EWs on final diagrams, shown in Fig. 6, to better see the trends.

For the Hα line we found that EW changes from 2.50 to 2.85 Å over an orbital phase (see Fig. 6). The average value of 2.70 Å agrees very well, within the uncertainties, with the result of C05 (2.8 ± 0.1 Å), except they found that the value was stable during the orbit of the binary (which could possibly be explained by the relatively low resolution of their spectra). Our result is also consistent with the EW values measured by others over the last 10 yr (Bosch-Ramon et al. 2007). Using the method of Puls et al. (1996) we estimated the mass-loss rate from the EW of the Hα line. To do these calculations we adopted the following parameters: $R_O = 9.3^{+0.7}_{-0.6}\,R_\odot$ and $T_{\rm eff} = 39\,000 \pm 1000$ K for the O-type star (C05); a terminal wind velocity of $V_\infty = 2440 \pm 190\,{\rm km\,s^{-1}}$ with a wind velocity law exponent of $\beta = 0.8$ (M04). We found that the mass-loss rate of the stellar companion is around $3.7 \times 10^{-7}\,M_\odot\,{\rm yr^{-1}}$ from the strongest absorption, which corresponds to the lower limit, and

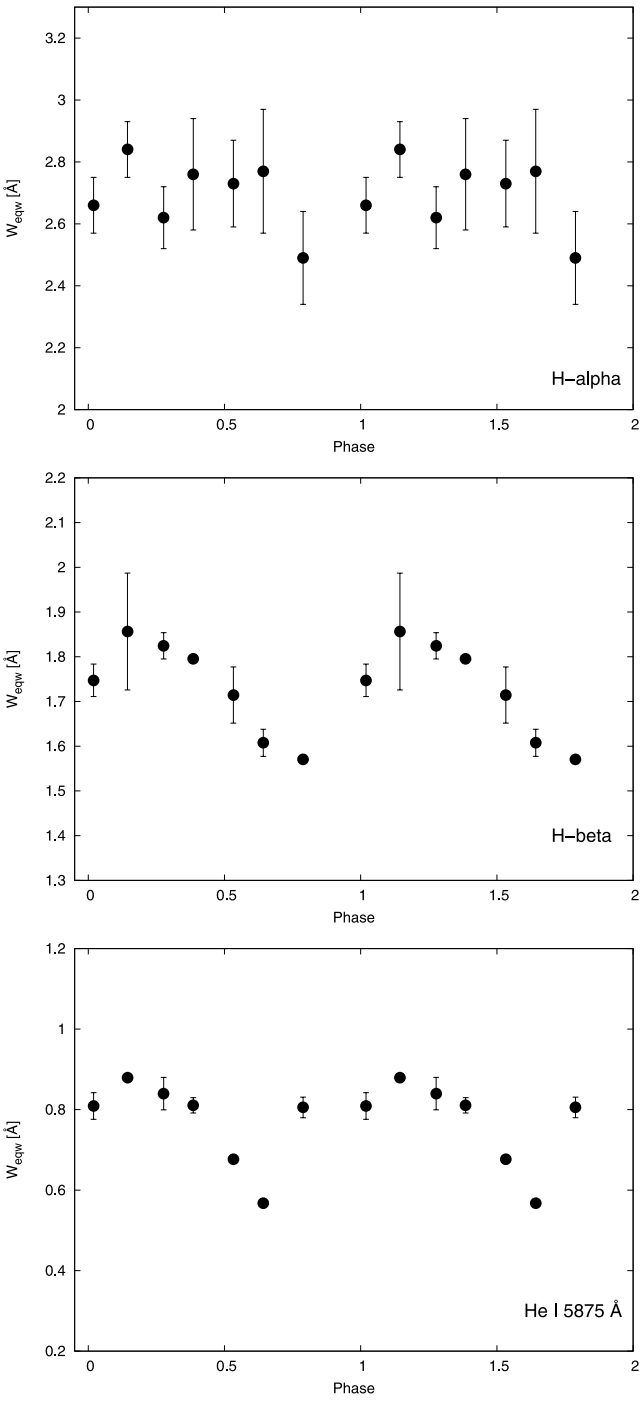

Figure 6. Variability of EW of Hα, Hβ and He I λ5875 absorption lines during the orbit. The mean values and the given error bars of points were calculated from results we got from three different methods (direct measurement with IRAF splot task, and fitting Gaussian or Lorentzian curve to the line profile) used to determine EWs of lines.

$4.8 \times 10^{-7}\,M_\odot\,{\rm yr^{-1}}$ for the upper limit. These values are consistent with the mass-loss rates of $\approx 3.7 \times 10^{-7}\,M_\odot\,{\rm yr^{-1}}$ for the low state (strong absorption) and $\approx 7.5 \times 10^{-7}\,M_\odot\,{\rm yr^{-1}}$ for the high state obtained by C05 (see also M04).

We found two lines (Hβ and He I λ5875) showing significant changes during the orbit. The lowest absorption for the Hβ line occurs around $\varphi \sim 0.75$, and at $\varphi \sim 0.65$ for the He I line (Fig. 6), close to the expected phase $\varphi \sim 0.7$ when the compact object is

between us and the stellar companion (inferior conjunction). The lower EW at inferior conjunction implies an increased emission strength likely due to the focusing of the stellar wind toward the compact object. Models of the wind flow in the system will need to take that focusing into account, especially those that model a pulsar wind/stellar wind interaction. We carried out a simple correlation analysis between these EW changes and the *MOST* light curve (rebinned to the EW bin size), and found the correlation coefficients, r, to be 0.52, 0.70 and 0.52 for the Hα, Hβ and He I λ5875 lines, respectively. This result suggests the possibility of real modulations over the orbital period, but further studies are necessary.

Note that our data only show smooth orbital modulation in the Hα, Hβ and He I absorption lines and in the emission components of the H Balmer lines. The lines do not show evidence of dense clump-like condensates in the stellar wind.

3.5 Some remarks

The two main findings from our work are that the orbit has a significantly lower eccentricity than previously thought and that the total mass of the system is toward the higher end of previous estimates, when the variability of the *MOST* data is considered. We were not able to resolve the nature of the compact object, between neutron star and black hole, in spite of simulations by C05 that postulated that a low-amplitude light curve would be associated with a low inclination and a black hole. The eccentricity $e \approx 0.4$ obtained by M04 put LS 5039 as the system with the most eccentric orbit among X-ray binaries with an O donor star. Although the value was later shown to be lower ($e \approx 0.35$, C05 and A09), the eccentricity would still be high enough to have some consequences on the dynamical and radiative properties, and on the evolutionary history, of the system. The observed TeV spectrum is consistent with inverse Compton scattering from electrons distant from the compact object either in a pulsar wind/stellar wind shock if the compact object is a neutron star, or in a jet if the compact object is a black hole. The lack of accretion features in the X-ray spectrum favours the pulsar model unless the bulk of the accretion power is released as kinetic energy in jet outflow instead of thermally from an accretion disc (Takahashi et al. 2009). In either case the keV X-rays are hypothesised to originate as synchrotron emission from the electrons responsible for the inverse Compton TeV emission. This is in contrast to the canonical view of X-ray emission from X-ray binaries. In the canonical view, the keV X-rays from X-ray binaries with an O star are powered by the accretion of gas either in a wind focused by the Roche lobe of the donor star or captured directly from the wind outflowing from the donor star. In the focused wind scenario, an accretion disc is expected to form around the compact star, similar to that in systems with Roche lobe filling mass transfer, as the accreting gas carries substantial specific angular momentum. In the direct wind capture scenario, provided that the specific angular momentum of the gas is sufficiently small, an extensive accretion disc might not be formed and the accretion inflow would be practically radial and resemble that of a Bondi–Hoyle flow. A lower orbital eccentricity would give a lower specific angular momentum in the wind material that is swept up by the accreting star. So far observations [e.g. X-ray observations by *Chandra* and *XMM–Newton* (Martocchia et al. 2005; Bosch-Ramon et al. 2007)] have not shown evidence of an accretion disc in LS 5039. If LS 5039 has an extremely high orbital eccentricity as originally measured, the lack of an accretion disc around its compact star would need certain non-trivial explanations (cf. the situation in the Be X-ray binaries). The lower eccentricity may ease the situation somewhat, allowing radial gas inflow for a substantial distance before reaching the compact accretor. Then, if there is an accretion disc, it would not be expected to be a large and dense disc because such a disc would generate significant thermal soft keV X-rays, which are not detected in the *Chandra*, *XMM–Newton* and other X-ray observations. Our smaller value of eccentricity reduces the discrepancy between the low observed X-ray variability and what would be expected from wind accretion with Bondi–Hoyle like radial inflow [Bondi & Hoyle (1944), Bosch-Ramon et al. (2005), C05].

Known black hole high-mass X-ray binaries tend to have small orbital eccentricity, unlike the X-ray pulsars (see Liu, van Paradijs & van den Heuvel 2005; Liu et al. 2006; Liu, van Paradijs & van den Heuvel 2007). X-ray binaries with a black hole and an O donor star are very rare, and Cyg X–1 is the currently only known system in the Milky Way. The confirmation of LS 5039 as a black hole high-mass X-ray binary in which a massive O donor star and a black hole revolve around each other in an eccentric orbit would have important implications on how such systems are formed and how massive binaries evolve. In LS 5039, the compact star's progenitor, at a certain stage, should be more massive than the current O donor star, otherwise it would not have evolved to form the compact star. O stars have very short life spans ($\sim$ a few Myr), thus LS 5039 as an X-ray binary must be younger than a few million years. This is supported by the fact that LS 5039 has a highly eccentric binary orbit, which has yet to be circularized from a presumed recent supernova event. However, it is unclear whether the progenitor of the O star or the progenitor of the compact star had the larger initial mass, as a rapid evolution of the progenitor of the compact star could well be triggered by a mass transfer process, in which the system was compact enough to allow the progenitor of the current O star to overfill its Roche lobe and transfer material to the progenitor of the compact star. [For more on the evolution of very massive binaries, see e.g. Dalton & Sarazin (1995); Van Bever & Vanbeveren (2003); Dionne & Robert (2006).] If LS 5039 was indeed formed through this mass-transfer channel, a finding that it contains a black hole among the fewer than 200 known high-mass X-ray binaries in the Milky Way would imply that a black hole high-mass X-ray might be formed in close massive binaries more easily than previously thought. Young stellar clusters in star-forming galaxies may well be populated by LS 5039-type sources and are potentially GeV–TeV γ-ray sources.

4 CONCLUSIONS

Our simultaneous optical photometry from the *MOST* space telescope and high-resolution echelle optical spectroscopy from the ANU 2.3-m Telescope have put further constraints on the orbital parameters of the LS 5039 system. In particular we obtained a mass function $f(m) \approx 0.0049 \pm 0.0006\,\mathrm{M}_\odot$ and an orbital eccentricity $e = 0.24 \pm 0.08$. The maximum photometric variation of LS 5039 in the *MOST* light curve was 2 mmag. The low photometric variation is consistent with the lower orbital eccentricity of 0.24, as opposed to the value of 0.35 found by others, and it is consistent with a higher overall system mass. However, we cannot determine the inclination on the basis of the low photometric amplitude. Our light curve simulations imply that the mass of the compact object is at least $1.8\,\mathrm{M}_\odot$ based on an inclination of 60° or less. Our value for the eccentricity of 0.24 ± 0.08 is a little smaller than previous determinations. The lower eccentricity implies that the wind material that is captured and falls into the Roche lobe of the compact star has a lower specific angular momentum. Thus it may not lead to the formation of a large-scale optically thick accretion disc,

and the accretion inflow is practically radial resembling that of a Bondi–Hoyle flow. This radial inflow would explain the lack of an accretion disc signature in keV data and should be considered in models of mass transfer for either a non-accreting pulsar or a black hole. Finally from EW measurements of the Hα line, we derived that the mass-loss rate from the O-type primary through stellar wind is 3.7 to 4.8 $\times$ 10^{-7} $M_{\odot}$ yr^{-1}, similar to values obtained by other workers. Our observations do not show evidence of dense clumps in the stellar wind.

ACKNOWLEDGMENTS

This work has been supported by the Australian Research Council, the University of Sydney, the Hungarian OTKA Grants K76816 and MB0C 81013, and the 'Lendület' Young Researchers' Programme of the Hungarian Academy of Sciences. KW's visits to Sydney University were supported by the University of Sydney International Visiting Fellowship.

REFERENCES

Abdo A. A. et al., 2009, ApJ, 706, L56
Acciari V. A. et al., 2008, ApJ, 679, 1427
Aharonian F. A. et al., 2005a, Sci, 309, 746
Aharonian F. A. et al., 2005b, A&A, 442, 1
Aharonian F. A. et al., 2006, A&A, 460, 743
Albert J. et al., 2006, Sci, 312, 1771
Albert J. et al., 2007, ApJ, 665, L51
Aragona C., McSwain M. V., Grundstrom E. D., Marsh A. N., Roettenbacher R. M., Hessler K. M., Boyajian T. S., Ray P. S., 2009, ApJ, 698, 514 (A09)
Araudo A. T., Bosch-Ramon V., Romero G. E., 2009, A&A, 503, 673
Bondi H., Hoyle F., 1944, MNRAS, 104, 273
Bosch-Ramon V., 2010, in Martí J., Luque-Escamilla P. L., Combi J. A., eds, ASP Conf. Ser. Vol. 422, High Energy Phenomena in Massive Stars. Astron. Soc. Pac., San Francisco, p. 77
Bosch-Ramon V., Paredes J. M., Ribó M., Miller J., Reig P., Martí J., 2005, ApJ, 628, 388
Bosch-Ramon V., Motch C., Ribó M., Lopes de Oliveira R., Janot-Pacheco E., Negueruela I., Paredes J., Martocchia A., 2007, A&A, 473, 545
Bosch-Ramon V., Khangulyan D., Aharonian F. A., 2008, A&A, 489, L21
Casares J., Ribó M., Ribas I., Paredes J., Martí J., Herrero A., 2005, MNRAS, 364, 899 (C05)
Cerutti B., Dubus G., Henri G., 2008, A&A, 488, 37
Clark J. S. et al., 2001, A&A, 376, 476
Cox N. L. J., Kaper L., Foing B. H., Ehrenfreund P., 2005, A&A, 438, 187
Dalton W. W., Sarazin C. L., 1995, ApJ, 448, 367
Dionne D., Robert C., 2006, ApJ, 642, 252
Dubus G., 2006, A&A, 456, 801
Dufton P. L. et al., 2006, A&A, 457, 265
Hinton J. A. et al., 2009, ApJ, 690, L101
Khangulyan D., Aharonian F. A., Bosch-Ramon V., 2008, MNRAS, 383, 467
Kishishita T., Tanaka T., Uchiyama Y., Takahashi T., 2009, ApJ, 697, L1
Lattimer J. M., Rakash M., 2007, Phys. Report, 442, 109
Liu Q. Z., van Paradijs J., van den Heuvel E. P. J., 2005, A&A, 432, 1135
Liu Q. Z., van Paradijs J., van den Heuvel E. P. J., 2006, A&A, 455, 1165
Liu Q. Z., van Paradijs J., van den Heuvel E. P. J., 2007, A&A, 469, 807
Lenz P., Breger M., 2004, in Zverko J., Ziznovsky J., Adelman S.J., Weiss W.W., eds, Proc. IAU Symp. 224, The A-Star Puzzle. Slovakia. Kluwer, Dordrecht, p. 786
McSwain M. V., Gies D. R., Riddle R. L., Wang Z., Wingert D. W., 2001, ApJ, 558, L43
McSwain M. V., Gies D. R., Huang W., Wiita P. J., Wingert D. W., Kaper L., 2004, ApJ, 600, 927 (M04)
Martí J., Paredes J. M., Ribó M., 1998, A&A, 338, L71
Martins F., Schaerer D., Hillier D. J., 2005, A&A, 436, 1049
Martocchia A., Motch C., Negueruela I., 2005, A&A, 430, 245
Matthews J. et al., 1999, J. Royal Astron. Soc. Canada, 93, 183
Motch C., Haberl F., Dennerl K., Pakull M., Janot-Pacheco E., 1997, A&A, 323, 835
Munari U., Zwitter T., 1997, A&A, 318, 269
Paredes J. M., Martí J., Ribó M., Massi M., 2000, Sci, 288, 2340
Paredes J. M., Ribó M., Ros E., Martí J., Massi M., 2002, A&A, 393, L99
Puls J. et al., 1996, A&A, 305, 171
Ribó M., Paredes J. M., Romero G. E., Benaglia P., Martí J., Fors O., García-Sánchez J., 2002, A&A, 384, 954
Ribó M., Paredes J. M., Moldón J., Martí J., Massi M., 2008, A&A, 481, 17
Sierpowska-Bartosik A., Torres D. F., 2007, ApJ, 671, L145
Takahashi T. et al., 2009, ApJ, 697, 592
Tavani M. et al., 2009, Nat, 462, 620
Van Bever J., Vanveveren D., 2003, A&A, 440, 63
Wakker B. P., van Woerden H., 1997, ARA&A, 35, 217
Walker G. et al., 2003, PASP, 115, 1023
Wilson R. E., 1994, PASP, 106, 921
Wilson R. E., Devinney E. J., 1971, ApJ, 166, 605
Wilson R. E., van Hamme W., 2003, Computing Binary Stars Observables. Ver. 4. Univ. Florida, Gainesville, preprint

This paper has been typeset from a TEX/LATEX file prepared by the author.